ORIGINAL ARTICLE

Hydrochemistry and geothermometry of geothermal water in the central Guanzhong Basin, China: a case study in Xi'an

Panpan Xu[1,2] · Mengna Li[1,2] · Hui Qian[1,2] · Qiying Zhang[1,2] · Fengxia Liu[1,2] · Kai Hou[1,2]

Abstract

The Xi'an geothermal field is a typical medium–low-temperature group of geothermal reservoirs in the Guanzhong Basin. Three distinct groundwater systems occur in this field: the cold groundwater (CG) system (quaternary cold-water reservoir with a depth of less than 300 m); the shallow geothermal water (SGW) system (the Quaternary, Zhangjiapo Group, and Lantian-Bahe Group thermal reservoirs with depths ranging between 300 and 2000 m); the deep geothermal water (DGW) system (the Gaoling Group, Bailuyuan Group, and Proterozoic crystalline rock fissure thermal reservoirs, with depths of more than 2000 m). The chemical composition of the CG system consists of HCO_3–Ca and HCO_3–Ca–Mg water types with a low Total Dissolved Solids' (TDS) content. The chemical composition of the SGW system consists of SO_4–Na and SO_4–HCO_3–Na water types that have resulted from the partial mixing with water from the CG system through fault structures. Calculations suggest that about 39.4–42.7% of the water in the SGW system was derived from the CG system. The chemical composition of the DGW system consists of SO_4–Na and SO_4–Cl–Na water types with elevated TDS, F^-, SiO_2, and high ion concentrations due to the long residence time of water in this largely closed system. The use of geothermometers, multiple mineral equilibrium calculations, and the silica-enthalpy mixing model suggests that temperatures in the SGW and DGW systems lie in the range of 40–85 °C and 94.7–135 °C, respectively. The chalcedony geothermometer is considered to provide the most reliable temperature estimates of the shallow reservoir, whereas the quartz[b] (maximum steam loss 100 °C) and Na–K geothermometers are considered to provide the most reliable estimates for the deep thermal reservoir. The results of a Q-cluster classification of the water agree well with the field classification of the sampled waters, and the associations of the principal variables obtained by the R-cluster method are consistent with the results obtained by the conventional hydrogeochemical assessment of the samples.

Keywords Geothermometry · Hydrogeochemistry · Mixing processes · Xi'an geothermal water · Guanzhong Basin

Introduction

Geothermal resources have been extensively developed and utilized globally in recent decades, for both environmental and economic reasons (Guo et al. 2017; Karimi et al. 2017; Lund and Boyd 2016; Sanada et al. 2006; Yang et al. 2017).

✉ Hui Qian
  qianhui@chd.edu.cn

[1] School of Environmental Science and Engineering, Chang'an University, No. 126 Yanta Road, Xi'an 710054, Shaanxi, China

[2] Key Laboratory of Subsurface Hydrology and Ecological Effects in Arid Region of the Ministry of Education, Chang'an University, No. 126 Yanta Road, Xi'an 710054, Shaanxi, China

Geothermal resources, comprising heat, minerals, and water, have been widely used for greenhouses, geothermal heating, hot spring bathing, and other therapeutic purposes, and are one of the most practical and competitive clean-energy sources for mitigating global climate change (Karimi et al. 2017; Lu et al. 2018; Michael et al. 2010). Geothermal resources are widely distributed about China and have long been exploited, with the Guanzhong Basin being a typical example.

The Guanzhong Basin is rich in geothermal resources and has a long history of exploitation. As early as the Western Zhou Dynasty (eleventh century to 771 BC), geothermal resources in the region were used by ancient peoples for medicinal bathing. The most famous example is the Huaqingchi hot spring in the Lintong district, east of Xi'an City (Qin et al. 2005b). Xi'an serves as the capital of Shaanxi

Province, and the Xi'an geothermal system is representative of the geothermal systems in the central Guanzhong basin. Although there have been a number of studies on the geochemical characteristics, recharge–flow–discharge conditions, and water–rock interactions on the basis of the geology, hydrogeology, and hydrogeochemistry in the Xi'an geothermal field (Ma et al. 2017; Qin et al. 2005a, b), a few studies have estimated the reservoir temperatures at different depths in this region. Therefore, to meet this need, this paper qualitatively and quantitatively studies the Xi'an geothermal field by combining a comprehensive geothermometric investigation with a multivariate statistical analysis of the results.

Combining results from a range of geothermometric methods, including various geothermometers, a multiple mineral equilibrium approach, and the silica-enthalpy mixing model, can enable a reasonable evaluation of geothermal reservoir temperatures. The most common silica geothermometers are quartz (Fournier 1977; Fournier and Potter 1982) and chalcedony (Morey et al. 1962), while Na–K–Ca (Fournier and Truesdell 1973), Na–K, and K–Mg (Giggenbach 1988) are the most commonly used cation geothermometers. These geothermometers have been widely applied for estimating the temperatures of geothermal systems. However, due to the major drawback of being unable to judge the equilibrium status of the studied systems, different geothermometers often give different temperatures (Pang 2001).

The multiple mineral equilibrium method has the advantage of acquiring a specific geothermal reservoir temperature on the basis of the equilibrium states of the minerals present (Avsar et al. 2013; Palandri and Reed 2001). However, the potential effects of a modern hydrological cycle often produce hydrogeological conditions in a shallow geothermal reservoir that are not favorable for an equilibrium state to be reached (Adam and Jan 2008). In addition, in deep geothermal systems, the erroneous interpretations of geothermal reservoir temperatures can be caused by the gain or loss of steam (Arnórsson 1983; Ben Brahim et al. 2014). The silica-enthalpy mixing model has been applied to calculate the mixing ratios and reservoir temperatures of geothermal systems at different depths (Guo et al. 2017; Liu et al. 2015; Reed and Spycher 1984). Therefore, using the methods described above in combination can provide a sound means of obtaining reliable reservoir temperatures.

Multivariate statistical techniques, such as cluster analysis (CA), factor analysis (FA), and principal components analysis (PCA), are effective, quantitative, and independent tools for classifying groundwater into different groups, assessing groundwater quality, and interpreting the relationship between the hydrochemistry and origin of geothermal water (Ben Brahim et al. 2014; Cloutier et al. 2008; Dassi 2011; Foued et al. 2017; Liu et al. 2008; Mondal et al. 2010; Zhang et al. 2014). Of the above-mentioned methods, CA is the most suitable and commonly used technique for grouping

entities or items into unknown groups (Foued et al. 2017). Its principle is that the highest similarity and lowest difference between samples in a group can be achieved based on a plurality of statistical indicators. Swanson et al. (2001) used two-way cluster analysis to determine the source of spring water based on geochemical data. Guo and Wang (2012) used CA and *t* test analysis to obtain preliminary evidence for the existence of a parent geothermal reservoir below the Rehai geothermal field. Zhang et al. (2014) classified groundwater in a heavily used semi-arid region and the natural and/or human factors affecting its composition through the use of Q-cluster analysis and R-cluster analysis. Foued et al. (2017) used Q-cluster analysis to define three main groups of springs reflecting different hydrochemical processes. Hence, the combined utilization of CA and hydrochemical methods has the potential to shed light on the characteristics of thermal and cold groundwater and the temperatures of deep and shallow geothermal systems in Xi'an.

The aim of this paper is to study the hydrochemistry of the thermal waters, identify the processes affecting the geothermal water compositions, and give a reliable estimation of the geothermal reservoir temperatures at different depths in the Xi'an geothermal field by applying statistical, geochemical, and geothermometric methods. The results of this research are intended to provide clear guidance for the sustainable development and utilization of the geothermal resources of the Xi'an geothermal field, and for the Guanzhong Basin as a whole.

Physical characteristics of the study area

Location and climate

The Guanzhong Basin is located between latitudes 106°30′ and 110°30′E, and longitudes 33°00′ and 35°20′N in Shaanxi Province, China. It covers an area of 2×10^4 km^2 and has an average elevation of 400 meters above sea level (m.a.s.l). It is a Cenozoic fault-block basin, predominantly filled with Tertiary fluvial and aeolian sediments and Quaternary loess (Qin et al. 2005b). It is bounded by the Qinling Mountains to the south, the Baoji Canyon to the west, the North Mountains to the north, and is open to the east. The Wei River, the largest tributary of the Yellow River, traverses the Guanzhong Basin. Tributaries originating from the Qinling Mountains are densely distributed on the south bank of the Wei River and serve as a source of groundwater recharge (Fig. 1). The Xi'an geothermal field mainly lies between the south bank of the Wei River and the Qinling Mountains, and covers an area of about 1300 km^2 (Qin et al. 2005b).

Local meteorological data indicate that the study area has a warm temperate semi-humid continental monsoon climate with an average annual temperature of 13.7 °C and average
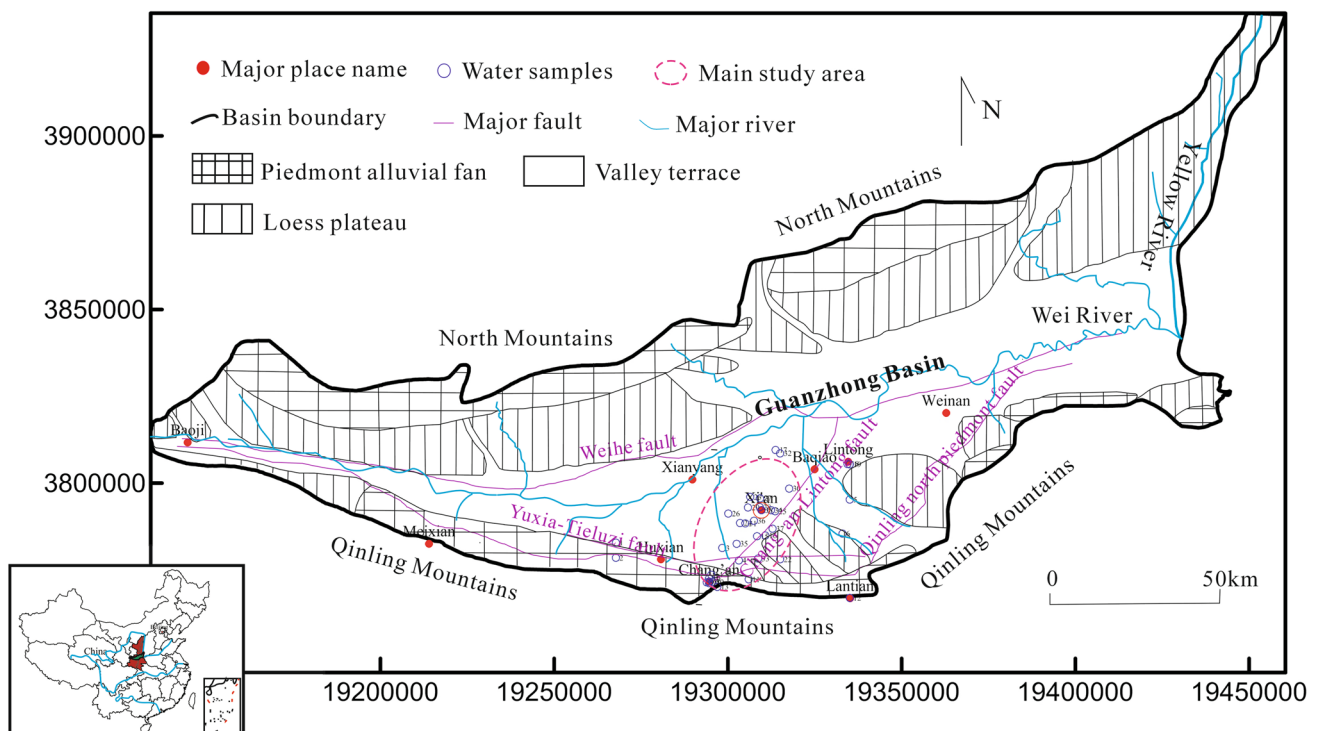
Fig. 1 Simplified geographic map and sampling locations of the Xi'an geothermal field, Guanzhong Basin, China (compiled from: Ma et al. 2017)

annual precipitation of 569.6 mm. From the mountain to the center of the basin, the terrain can be characterized, sequentially, as the Qinling Mountains, piedmont alluvial fan, loess plateau, and valley terrace (Fig. 1).

Geological setting

There are three significant faults in the Xi'an geothermal field: the NE–SW-stretching Chang'an-Lintong fault, the E–W-stretching Qinling North Piedmont fault, and the Yuxia-Tieluzi fault. These faults serve as discharge channels for the upward flow of geothermal fluids (Fig. 1). The largest discharges of geothermal water are associated with artificial extraction, followed by runoff and hot spring activity. The geothermal water in this region is generally recharged by runoff from the Qinling Mountains (Ma et al. 2017). The surface of the Guanzhong Basin is covered by Quaternary sediments, and the basement of the basin is divided into three zones by the Weihe and Chang'an–Lintong faults (Fig. 2). The Lower Paleozoic carbonate rocks are distributed in the northern part of the Weihe fault. The distribution of the Archean gneiss is from the Qinling Mountains in the east to the Chang'an–Lintong fault in the west, and from the Weihe fault zone in the north to the Yuxia-Tieluzi fault in the south. A Proterozoic schist is located in the area to the south of the Weihe fault zone and to the west of the

Chang'an–Lintong fault, with granitic rocks also outcropping in this area. The Xi'an geothermal field is mainly located in an area underlain by Proterozoic schists.

The Xi'an geothermal resources can be divided into three different types on the basis of geological structure, lithology, and geothermal occurrence. These are: an unconsolidated porous-medium Quaternary thermal reservoir; a Neoproterozoic and Paleogene clasolite pore-fissure thermal reservoir; and a Proterozoic crystalline rock fissure thermal reservoir. The total amount of geothermal heat in all reservoirs is 2.11×10^{16} kJ, and the volume of the geothermal water resources is about 5.47×10^8 m^3 (Jiang and Wu 2009).

As shown in Fig. 2, the regional hydrogeology, from the surface downwards, can be summarized as follows. The Quaternary sediment reservoir (Q) with an average geothermal temperature of 30–50 °C is easily exploited over depths of 300–700 m. The Neoproterozoic and Paleogene thermal reservoir can be subdivided into four groups [the Zhangjiapo Group (N_2z), the Lantian-Bahe Group (N_1l+b), the Gaoling Group (N_1gl), and the Bailuyuan Group (E_3b)] that have average geothermal temperatures of 40–70 °C, 50–90 °C, 80–120 °C and 130–150 °C, and depths of 500–1300 m, 900–1800 m, 1500–2400 m, and 2900–3100 m, respectively. A Proterozoic thermal reservoir (Pt_2) made up of bedrock crevices is located mainly within the Qinling North Piedmont fault zone, and has an average geothermal temperature
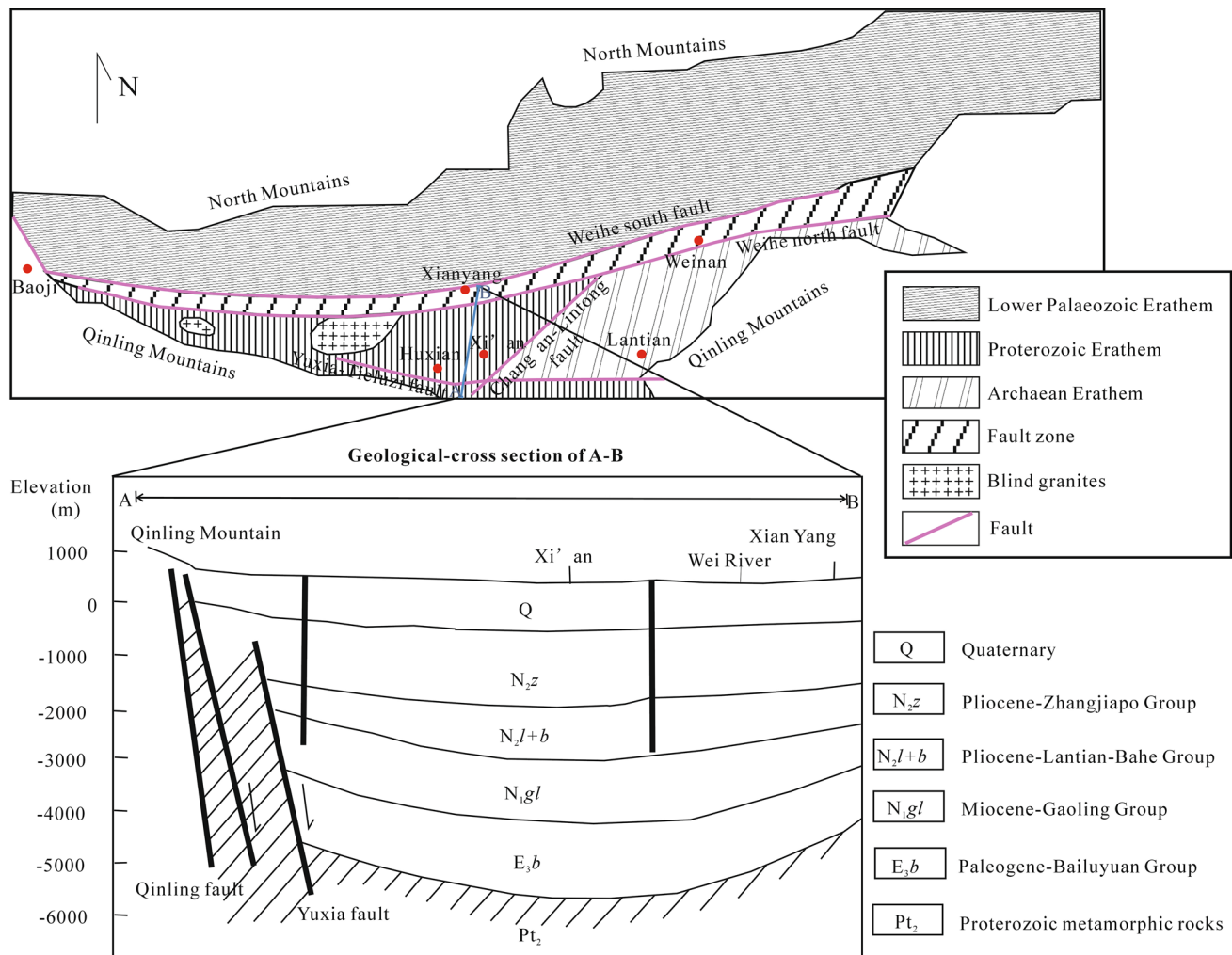
Fig. 2 Geological basement structure of the Guanzhong Basin and geological-cross section of study area (compiled from: Xu 2014)

and depth of more than 140 °C and 4000 m, respectively. The minerals identified in the reservoir rocks include analcite, Na-feldspar, calcite, quartz, fluorite, muscovite, chalcedony, anhydrite, and chrysotile (Qin et al. 2005b).

Sampling and assessment methods

A total of 38 water samples were collected in Xi'an, including six samples of cold groundwater (CG) from well depths ranging from 220.0 to 302.8 m in the Quaternary aquifer, 16 samples of shallow geothermal water (SGW) from well depths ranging from 292.4 to 1985.0 m in the Q, N_2z, and N_2l+b reservoirs, and 16 samples of deep geothermal water (DGW) from well depths ranging from 2350.0 to 4005.6 m in the N_2l+b, N_1gl, and E_3b reservoirs. The sampling locations are shown in Fig. 1, and the hydrochemical characteristics of the water samples are listed in Table 1. The water temperature, pH, and total dissolved solids (TDS) were tested immediately in

the field using a portable multiparameter meter (XS700) at the sampling point. Each sample was collected in two polyethylene bottles: one for cation analysis and the other for anion analysis. To prevent metal ions from reacting, the samples for cation analysis were acidified with pure nitric acid to pH < 2. After bottling, all water samples were stored at 4 °C for transport to the laboratory.

The concentrations of major cations (Na^+, K^+, Ca^{2+}, and Mg^{2+}) and SiO_2 were measured with an AA-100 atomic absorption spectrometer with a precision that varied from 2 to 5%. Anions (Cl^-, SO_4^{2-}, and F^-) were determined by ion chromatography with an analytical accuracy of less than 5%, and HCO_3^- was tested by alkalinity titration. The ion charge balance errors were calculated to be between −0.1 and 9.5%, with a mean value of 2.2%. The saturation indices (SI) for specific mineral phases were calculated using the Phreeqc Interactive 2.8 software, and the CA of the water samples was performed using the IBM SPSS Statistics 20 software package.

Table 1 Hydrochemical characteristics of water samples in the Xi'an geothermal field

Sample ID	Label	Well depth (m)	T (°C)	pH	TDS (mg/L)	K⁺ (mg/L)	Na⁺ (mg/L)	K⁺+Na⁺ (mg/L)	Ca²⁺ (mg/L)	Mg²⁺ (mg/L)	Cl⁻ (mg/L)	SO₄²⁻ (mg/L)	HCO₃⁻ (mg/L)	F⁻ (mg/L)	SiO₂ (mg/L)	CBE (%)	Water type
CG1	1	302	16	7.8	269.4	n.a	n.a	25.9	68.1	10.9	5.3	9.7	299	0.2	25	1.8	HCO$_3$–Ca
CG2	2	293.6	15	7.7	174.8	n.a	n.a	8.4	48.1	8.5	5	18.2	173.3	0.4	17	1.7	HCO$_3$–Ca–Mg
CG3	3	302.8	21.5	7.9	276.1	n.a	n.a	44.7	62.1	4.2	7.1	20.7	274.6	0.1	22.5	2.5	HCO$_3$–Ca
CG4	4	302.8	16.5	7.7	325.9	n.a	n.a	36.9	62.1	23.1	12.4	14.4	353.9	0.1	18	1.4	HCO$_3$–Ca–Mg
CG5	5	220	20.5	7.5	273.6	n.a	n.a	8.7	66.7	20.8	9.9	29.3	276.4	0.1	23	0.2	HCO$_3$–Ca–Mg
CG6	6	256	23.5	7.3	301.1	n.a	n.a	13.3	75.8	21.8	1.8	6.2	364.3	0.3	15	0.3	HCO$_3$–Ca–Mg
SGW1	7	498	70	7.9	413.3	1.5	136.2	137.7	6	0.6	30.1	170.5	112.9	12	46.3	3.6	SO$_4$–HCO$_3$–Na
SGW2	8	514.5	68	8.1	297.3	1	98.5	99.5	5	0.6	21.3	105.7	115.9	7.2	45.7	–1	SO$_4$–HCO$_3$–Na
SGW3	9	700	63	8.9	299.9	1.4	106.9	108.3	4	0	23	111.9	88.5	8.5	28.7	4.9	SO$_4$–HCO$_3$–Na
SGW4	10	292.4	34	8	392.1	23.2	93	116.2	16	19.6	31.6	127.3	140.9	11	21.1	9.4	SO$_4$–HCO$_3$–Na–Mg
SGW5	11	356.1	54	8.7	495.4	22	142	164	10.6	9.6	40.8	204.1	103.1	14.8	32.1	6.4	SO$_4$–HCO$_3$–Na
SGW6	12	627.1	57	8.6	570.1	34.4	137.4	171.8	14	19	21.3	309.8	43.9	12.3	70.4	8	SO$_4$–Na
SGW7	13	581	61	8.5	460.1	5.5	160	165.5	8	0	34.1	184.9	111.1	12	76.4	6.1	SO$_4$–HCO$_3$–Na
SGW8	14	1370	52	8.3	403.8	1	143.2	144.2	3	0.6	63.8	122.5	115.9	11.7	23.9	1.6	SO$_4$–HCO$_3$–Cl–Na
SGW9	15	1500	55	8.2	555.6	2	213.8	215.8	3	0.6	28.4	180.1	238	8.7	30.3	6.1	HCO$_3$–SO$_4$–Na
SGW10	16	1890	57	8.1	801.9	2.8	284.4	287.2	7	0.4	30.1	332.8	274.6	7.1	25	2.1	SO$_4$–HCO$_3$–Na
SGW11	17	1352.5	40	7.7	1147.4	4.1	447.3	451.4	7	0.6	62	189.7	860.4	6.5	21.6	0.4	HCO3–Na

Table 1 (continued)

Sample ID	Label	Well depth (m)	T (°C)	pH	TDS (mg/L)	K^+ (mg/L)	Na^+ (mg/L)	$K^+ + Na^+$ (mg/L)	Ca^{2+} (mg/L)	Mg^{2+} (mg/L)	Cl^- (mg/L)	SO_4^{2-} (mg/L)	HCO_3^- (mg/L)	F^- (mg/L)	SiO_2 (mg/L)	CBE (%)	Water type
SGW12	18	865	52	8.1	783	61.5	296.5	358	19	4.2	203.8	259.4	378.3	3.7	21.1	−4.8	HCO_3–Cl–SO_4–Na
SGW13	19	1160	51	7.9	628.9	36.3	145.1	181.4	40.1	4.9	100.3	190.2	213.6	5.3	32.5	−3.2	SO_4–HCO_3–Cl–Na
SGW14	20	544	56	8.1	361.3	25	100	125	7	12.3	55.7	100.9	103.7	8.5	28.7	8.5	SO_4–HCO_3–Cl–Na
SGW15	21	950	83	8.3	422.3	2	143.2	145.2	8	1.8	39	156.1	122	11.2	46.2	3.6	SO_4–HCO_3–Na
SGW16	22	1985	55	8	498.3	1	187.2	188.2	4	0.4	40.8	78.3	366.1	3.6	26.9	−2.2	HCO_3–Na
DGW1	23	3004.3	95	7.3	3486.7	12.8	1149.5	1162.3	30.1	4.3	255.2	1416.9	1226.5	4.7	74.2	−4.3	SO_4–HCO_3–Na
DGW2	24	3854.5	102	8.3	5164.4	30	1725	1755	44.1	4.3	267.6	2545.6	1089.2	3.2	117.5	−0.1	SO_4–HCO_3–Na
DGW3	25	3004.6	94	7.3	4887	27.5	1587	1614.5	58.1	6.1	288.9	2569.9	689.5	4.8	70	0.1	SO_4–Na
DGW4	26	2618	93	7.8	1676.7	6	540.1	546.1	31.1	3	351	662.8	146.4	9.5	64	−1.3	SO_4–Cl–Na
DGW5	27	2651.7	99	7.7	3740	17.5	1340	1357.5	7	9.7	286.5	1438.5	1264.9	8.3	77.5	0.9	SO_4–HCO_3–Na
DGW6	28	2350	91	7.9	1860.4	8	659.2	667.2	15	0.6	324.4	638.8	414.9	6.9	46.2	0.7	SO_4–Cl–HCO_3–Na
DGW7	29	3000	91.5	7.8	1187.2	4.4	442.2	446.6	10	0	352.4	264.2	207.5	10.2	59.3	2.6	Cl–SO_4–Na
DGW8	30	3205.3	113	7.8	2210.9	14.5	763	777.5	14	0.6	281.8	734.9	793.2	5.5	63.5	−2.8	SO_4–HCO_3–Cl–Na
DGW9	31	3000	93	7.7	1770.6	5.6	610.8	616.4	29	0.6	329.7	696.4	177	10	41	2.7	SO_4–Cl–Na
DGW10	32	3305	95	7	5049.5	35	1846.3	1881.3	68.1	8.5	1595.2	1037.4	909.2	4.4	56.6	2.3	Cl–SO_4–Na
DGW11	33	3790	91	7.4	4155.4	28.2	1352.3	1380.5	125.2	18.2	372.2	2031.7	448.5	3.4	44	5.6	SO_4–Na

Table 1 (continued)

Sample ID	Label	Well depth (m)	T (°C)	pH	TDS (mg/L)	K^+ (mg/L)	Na^+ (mg/L)	$K^+ + Na^+$ (mg/L)	Ca^{2+} (mg/L)	Mg^{2+} (mg/L)	Cl^- (mg/L)	SO_4^{2-} (mg/L)	HCO_3^- (mg/L)	F^- (mg/L)	SiO_2 (mg/L)	CBE (%)	Water type
DGW12	34	3858	102	7.7	2454.1	21	825.6	846.6	34.1	2.4	170.2	1116.7	549.2	9.5	108.7	1.7	SO_4–HCO_3–Na
DGW13	35	3700.1	94	7.8	2111.8	4.4	701.6	706	29.1	1.8	131.2	1061.5	347.8	8.3	43.6	1.1	SO_4–Na
DGW14	36	4005.6	110	7.5	1724.9	14.5	610.8	625.3	20	0.6	326.1	600.4	286.8	9.1	48.1	2.9	SO_4–Cl–Na
DGW15	37	3450	98	7.4	2459.3	12.3	859.6	871.9	44.1	7.3	152.4	1335.2	82.7	7.1	68	9.5	SO_4–Na
DGW16	38	3000	91	7.9	1722.6	6	594.8	600.8	27.1	1.8	297.8	720.4	134.2	7.6	45.5	3.6	SO_4–Cl–Na

n.a. not analyzed

Results and discussion

Cluster analysis

The CA is based on Ward's clustering method, a metric of Euclidean distance, and the indicator variable data normalized over the interval [0,1]. It was performed on the complete set of water samples based on the hydrochemical compositions, as shown in Table 1. The Q-cluster method classifies the samples into clusters based on the similarity of their variables (Zhang et al. 2014). In this study, the Q-cluster method enabled the water samples to be divided into three groups: cluster 1 (SGW1-SGW16), cluster 2 (CG1-CG6), and cluster 3 (DGW1-DGW16), respectively (Fig. 3). Through the variance-ratio test, there are obvious differences among the three clusters, reaching the significant level of 0.05, which verifies the rationality of employing a clustering tendency.

The results of the Q-cluster analysis indicate that the water samples belonging to the three clusters had significantly different characteristics and so represent different categories of water. The mean concentrations of major ions are presented in Stiff diagrams for each cluster in Fig. 3. The composition of ions in the CG cluster was of the form $Ca^{2+} > Mg^{2+} > Na^+ + K^+$ and $HCO_3^- > SO_4^{2-} > Cl^-$. The order of the cationic and anionic concentrations for the SGW cluster was $Na^+ + K^+ > Ca^{2+} > Mg^{2+}$ and $SO_4^{2-} > HCO_3^- > Cl^-$. Similarly, the trend of the major cations and anions in the DGW cluster was $Na^+ + K^+ > Ca^{2+} > Mg^{2+}$ and $SO_4^{2-} > Cl^- > HCO_3^-$. It is likely that the differences in ionic composition described above were caused by different water–rock interactions, such as the processes involved in the dissolution of mineral phases, cation exchange, and mixing.

The R-cluster method is often used to assess associations among different variables (Zhang et al. 2014). In this study, the results of the R-clustering of seven variables ($Na^+ + K^+$, Ca^{2+}, Mg^{2+}, SO_4^{2-}, HCO_3^-, Cl^-, and TDS) for different water samples are shown in Fig. 4. In the CG samples, HCO_3^-, Ca^{2+}, and TDS were first clustered into a group, indicating that HCO_3^- and Ca^{2+} were predominant and the most significant contributors to the TDS, followed by Mg^{2+}. For the SGW samples, HCO_3^- and $Na^+ + K^+$ were contributors to the TDS, followed by SO_4^{2-}. In the DGW samples, $Na^+ + K^+$ and SO_4^{2-} were the dominant ions, followed by HCO_3^-. These results are consistent with the ion associations observed by plotting the chemical data on a Piper diagram, which is a commonly used tool for classifying the chemical composition of water samples (Li et al. 2016a, c; Piper 1944). Figure 5 shows that the CG samples have chemical compositions that plot in the HCO_3–Ca and HCO_3–Ca–Mg facies fields,
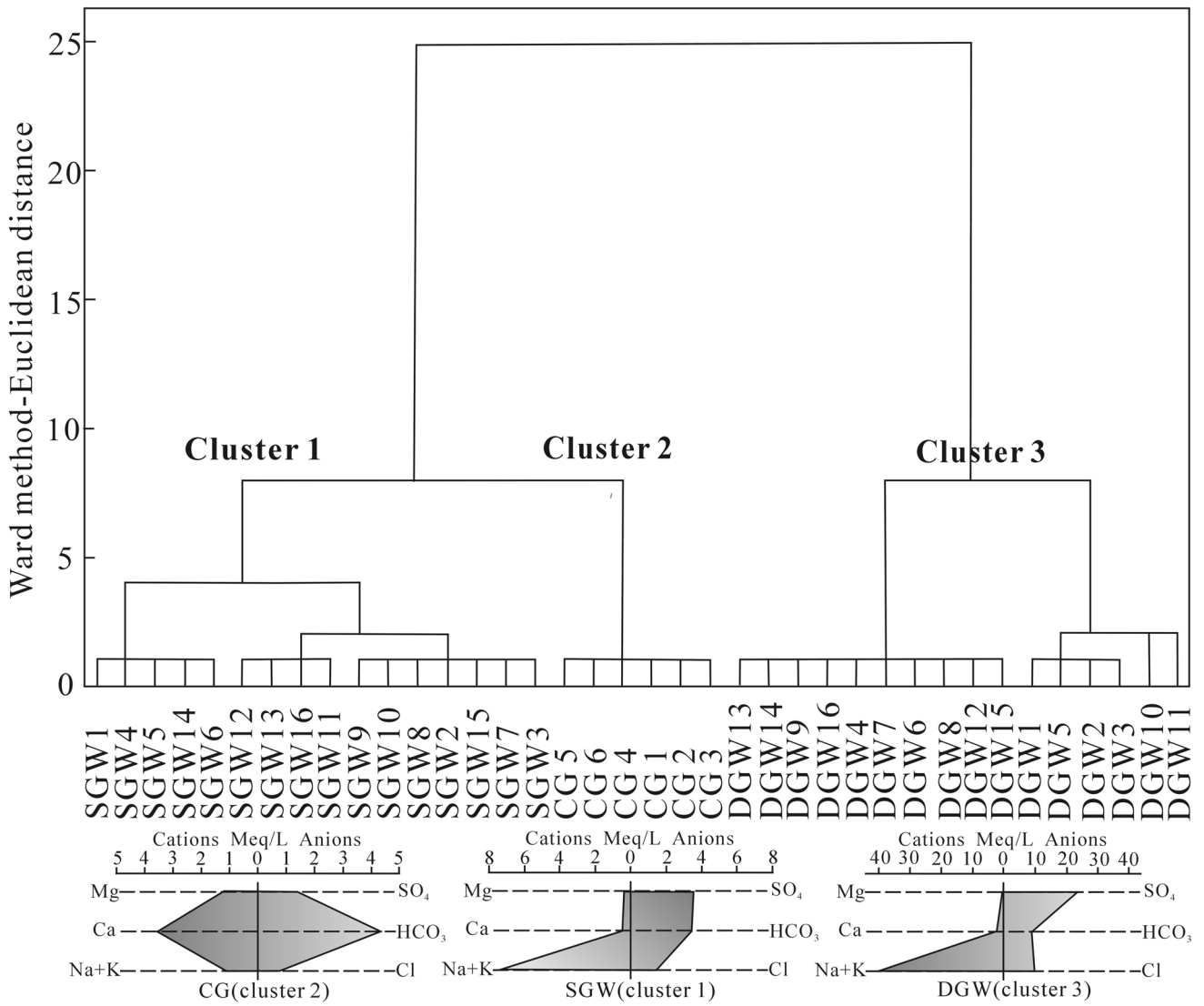
Fig. 3 Dendrogram from the Q-cluster analysis of all water samples and the Stiff diagram of mean concentrations for each cluster
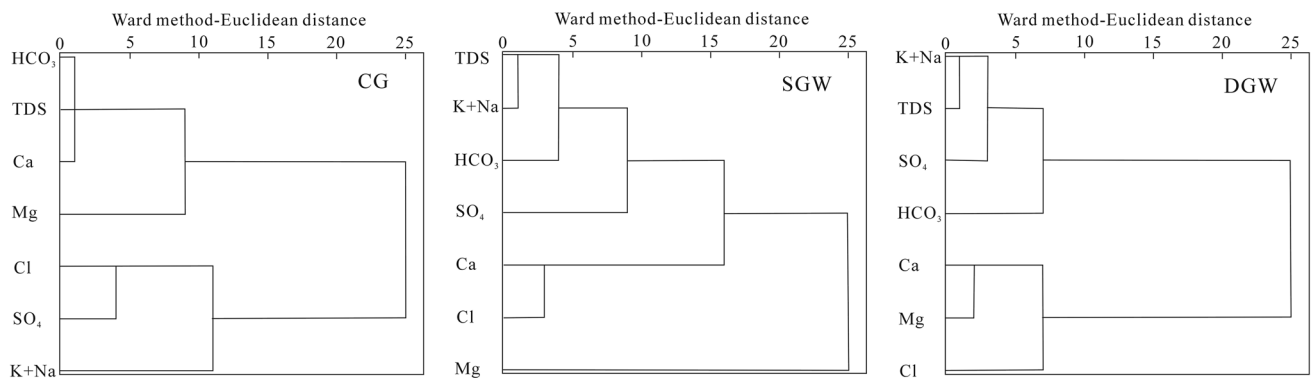

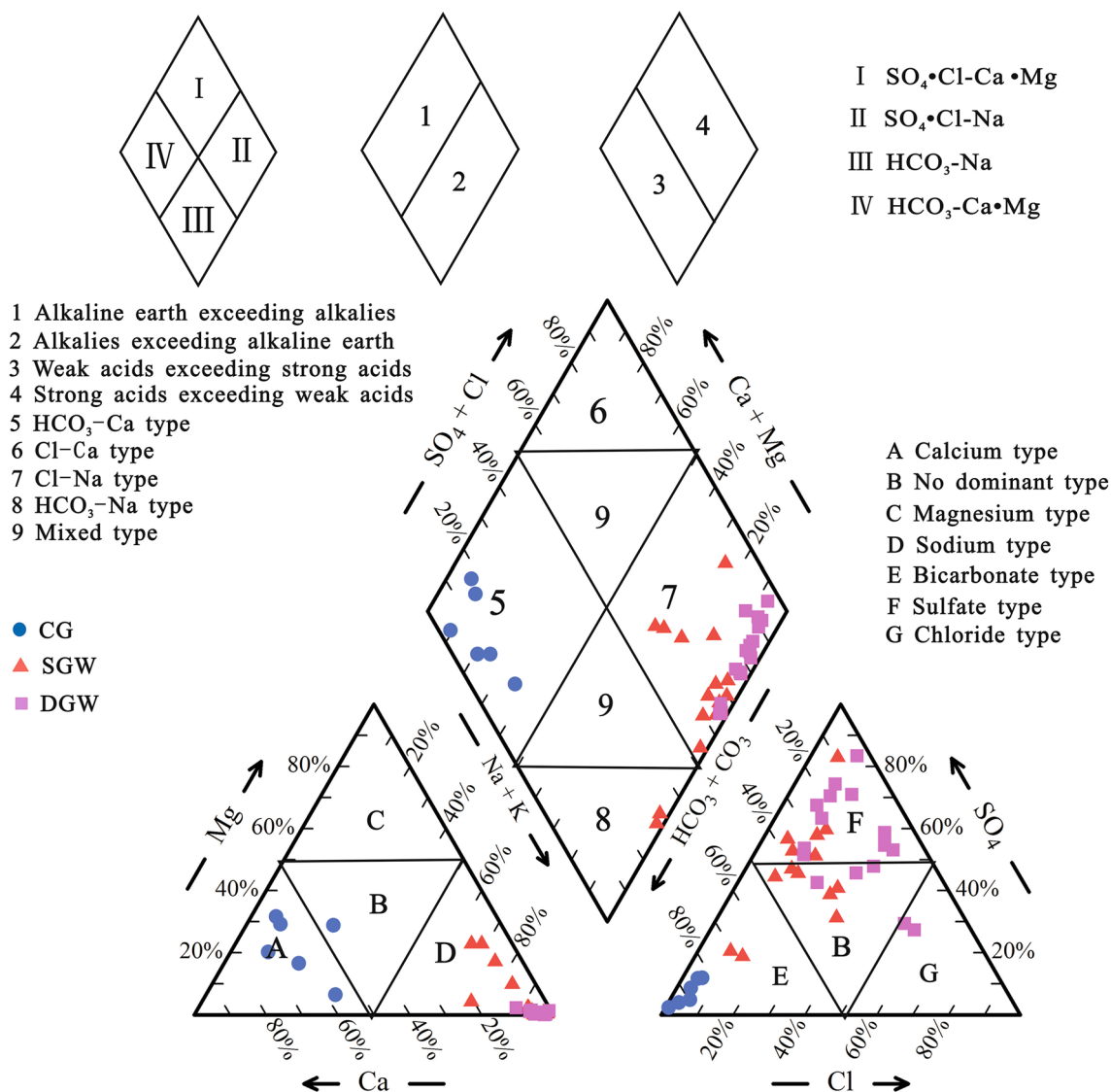**Fig. 4** Dendrogram from the R-cluster analysis of 7 variables for water samples from each of the geothermal systems

Fig. 5 Piper diagram of the water samples

whereas SO_4–HCO_3–Na is the dominant chemical composition in the SGW samples. Meanwhile, the DGW samples have chemical compositions that consist of SO_4–Na, SO_4–HCO_3–Na, and SO_4-Cl–Na water types.

Hydrogeochemical characteristics of the waters

As listed in Table 1, the temperature, TDS, and pH of the DGW samples ranged from 91 to 113 °C, 1187.2 to 5164.4 mg/L, and 7.0 to 8.3, with mean values of 97 °C, 2853.8 mg/L, and 7.6, respectively. The average concentrations of F^- and SiO_2 were 7.0 mg/L and 64.2 mg/L, respectively. For the SGW samples, the temperature, TDS, and pH ranged from 34 to 83 °C, 297.3 to 1147.4 mg/L, and 7.7 to 8.9, with mean values of 57 °C, 533.2 mg/L, and 8.2, respectively. The mean values of F^- and SiO_2 concentrations in

these samples were 9.0 mg/L and 36.1 mg/L, respectively. In contrast with the DGW and SGW samples, the mean TDS, F^-, and SiO_2 in the CG samples were relatively low, with average values of 270.1 mg/L, 0.2 mg/L, and 20.1 mg/L, respectively. The mean values of the temperature and pH of the CG samples were 19 °C and 7.7, respectively. The lower concentrations of major ions in the CG samples are attributed to the shorter transit pathways and shorter residence times of water in this aquifer system. In addition, water–rock interactions are often limited at shallow percolation depths (Chandrajith et al. 2013; Karimi et al. 2017).

Durov diagrams, which are useful for revealing the geochemical processes that have affected the groundwater components (Li et al. 2016b), have also been used in this study. This type of plot indicates that there is a change from water dominated by bicarbonate ions in the CG samples to
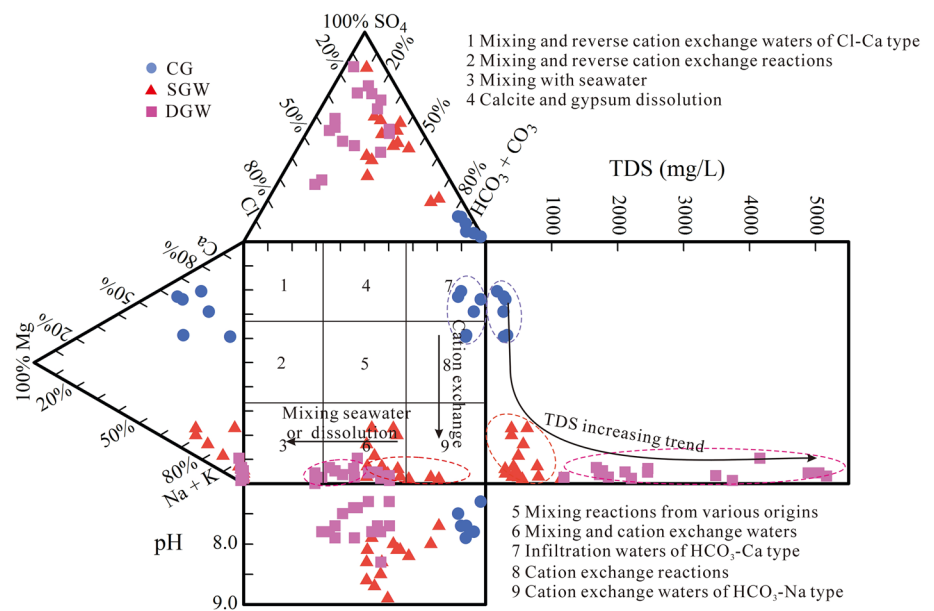
chloride or sulfate dominance in the SGW and DGW samples (Fig. 6), which is attributed to an increase in the duration of contact with the aquifer rocks. The geothermal water samples are mainly plotted in zones 6 and 9, suggesting that the SGW compositions probably evolved through mixing and cation exchange, and that the composition of the DGW samples had been subjected to more intensive water–rock interactions. The high HCO_3^- content in the SGW samples may have been derived from the dissolution of silicate and carbonate minerals. The CG samples are plotted in zone 7, which is consistent with the characteristics of modern infiltration water (Makni et al. 2013). In addition, all of the water samples were weakly alkaline, and there was a marked increase in the TDS from the CG and SGW to the DGW.

Ion ratios can be used to determine the origin of the water and to infer the hydrogeochemical processes that have influenced the chemical composition of a water body (Abdel Moneim et al. 2015). Relationships between the major ions can also be used to distinguish the different mechanisms that contributed to groundwater mineralization (Ben Brahim et al. 2014). In Fig. 7a, the Na/Cl ratio was greater than 1 for all samples, suggesting that the excess Na^+ could be mainly controlled by cation exchange and that this ion was not of marine origin in both the geothermal and CG systems. In Fig. 7b, the Ca/SO_4 ratios of all the geothermal water samples were small, but the magnitude of this ratio in the SGW samples was larger than that of the DGW samples. This suggests that the content of SO_4^{2-} in these waters was almost entirely controlled by anhydrite or gypsum dissolution, and that cation exchange reactions increase with the depth of the geothermal reservoir. The Ca/SO_4 ratio of the CG system was much larger than 1, which suggests that there are only limited water–rock interactions in this system.

As shown in Fig. 7c, d, the Ca/HCO_3 and $Ca + Mg/HCO_3$ ratios were much less than 1 and were similar in all water samples, suggesting that they had been affected by cation exchange, especially in the SGW and DGW samples. Similarly, Fig. 7e shows that the $Ca + Mg/HCO_3 + SO_4$ ratios of the SGW and DGW samples were less than 1 (although values of this ratio in the SGW samples are greater than those in the DGW samples), which also suggests that cation exchange reactions increase with the increasing depth of the geothermal reservoir. By contrast, the values of this ratio in the CG samples range between 0.70 and 0.99 with an average value of 0.87 (~ 1), which suggests that there are chemical interactions involving carbonates and sulfates and weak cation exchange in this system. Figure 7f indicates that the Ca/Mg ratio progressively decreases from the DGW, SGW to CG samples, which could be due to the effects of the different reservoir temperatures on the calcite–dolomite equilibrium where calcite incongruently dissolves and causes dolomite to precipitate.

The assessment of the correlations between the various chemical constituents in the water samples can be used to infer the geochemical processes that control the chemical composition of groundwater in an aquifer.

In this study, it was found the TDS had relatively high correlations with Ca^{2+}, Mg^{2+}, and HCO_3^- in the CG samples (Table 2), especially for HCO_3^-, where the correlation had a significance level of 0.01. This is likely to be due to the widespread distribution of carbonate minerals in the cold-water Quaternary aquifers. $Na^+ + K^+$ had a weakly positive correlation with Ca^{2+} and a negative correlation with Mg^{2+} in these aquifers, suggesting that the cation exchange was weaker here than in the SGW and DGW systems.
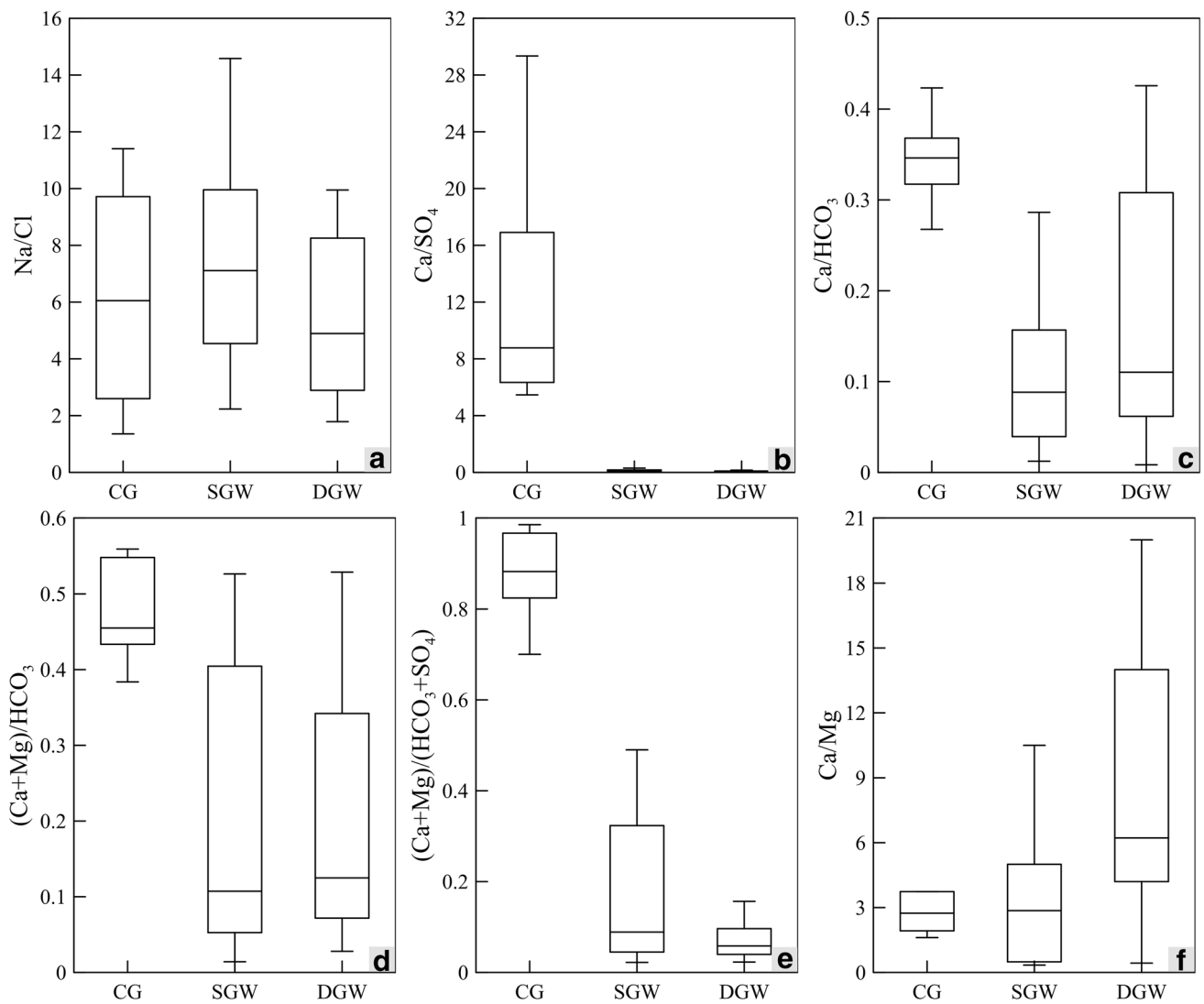
Fig. 7 Box–Whisker diagrams of ratios of the major elements in water samples

Table 2 Correlation matrix of the physico-chemical water parameters in CG

Catalog	$K^+ + Na^+$	Ca^{2+}	Mg^{2+}	Cl^-	SO_4^{2-}	HCO_3^-	pH	T	TDS	SiO_2	F^-
$K^+ + Na^+$	1										
Ca^{2+}	0.03	1									
Mg^{2+}	− 0.30	0.51	1								
Cl^-	0.38	− 0.22	0.29	1							
SO_4^{2-}	− 0.10	− 0.39	− 0.13	0.56	1						
HCO_3^-	0.33	0.83*	0.66	0.11	− 0.49	1					
pH	0.68	− 0.53	− 0.75	0.32	0.19	− 0.39	1				
T	0.02	0.68	0.22	− 0.29	0.02	0.47	− 0.52	1			
TDS	0.49	0.75	0.60	0.36	− 0.25	0.95**	− 0.21	0.45	1		
SiO_2	0.30	0.09	− 0.38	0.29	0.40	− 0.14	0.57	− 0.14	0.04	1	
F^-	− 0.51	− 0.30	− 0.19	− 0.76	− 0.51	− 0.36	− 0.27	− 0.19	− 0.62	− 0.65	1

*Significant at the 0.05 level (2-tailed)

**Significant at the 0.01 level (2-tailed)

Table 3 Correlation matrix of the physico-chemical water parameters in SGW

Catalog	K^+	Na^+	Ca^{2+}	Mg^{2+}	Cl^-	SO_4^{2-}	HCO_3^-	pH	T	TDS	SiO_2	F^-
K^+	1											
Na^+	0.00	1										
Ca^{2+}	0.70**	− 0.06	1									
Mg^{2+}	0.54*	− 0.42	0.31	1								
Cl^-	0.71**	0.40	0.49	− 0.14	1							
SO_4^{2-}	0.38	0.45	0.27	0.09	0.23	1						
HCO_3^-	− 0.05	0.91**	− 0.02	− 0.34	0.34	0.12	1					
pH	− 0.05	− 0.51*	− 0.29	0.09	− 0.28	0.00	− 0.67**	1				
T	− 0.33	− 0.24	− 0.27	− 0.47	− 0.15	− 0.03	− 0.38	0.43	1			
TDS	0.18	0.95**	0.19	− 0.22	0.42	0.59*	0.86**	− 0.55*	− 0.35	1		
SiO_2	− 0.07	− 0.26	− 0.02	0.02	− 0.30	0.23	− 0.40	0.41	0.49	− 0.22	1	
F^-	− 0.14	− 0.47	− 0.21	0.44	− 0.52*	0.04	− 0.56*	0.56*	0.06	− 0.41	0.39	1

*Significant at the 0.05 level (2-tailed)

**Significant at the 0.01 level (2-tailed)

Table 3 indicates that the TDS is positively correlated with major ion concentrations (except for Mg^{2+}) in the SGW samples, suggesting that water from the SGW system could have been mixed with water from the CG system, and, subsequently, have been re-equilibrated with the host rocks in the SGW system. The concentration of Na^+ was found to be negatively correlated with Ca^{2+} and Mg^{2+}, but positively correlated with HCO_3^- at the 0.01 significant level, suggesting that the dissolution of calcite and dolomite has a less significant influence on the chemical composition of the water than cation exchange.

Table 4 indicates that the concentrations of the major ions (Na^+, K^+, Ca^{2+}, Mg^{2+}, SO_4^{2-}, HCO_3^-, and Cl^-) in the DGW samples are positively correlated with the TDS. This is possibly due to the influence of the long residence time of water in this deep geothermal system, which has increased the importance of the water reactions with the aquifer's host rocks. Concentrations of Na^+ were also significantly and positively correlated with Ca^{2+} and Mg^{2+}, implying that the intense dissolution of gypsum, anhydrite, calcite, and dolomite provided sufficient Ca^{2+} and Mg^{2+} and promoted cation exchange. The correlation of Ca^{2+} with SO_4^{2-} was stronger than that of Ca^{2+} with HCO_3^-, so the dissolution of gypsum can be assumed to be a major source of Ca^{2+}. In addition, SiO_2 in the SGW and DGW samples was positively correlated with temperature, suggesting that geothermal reservoir temperatures can be predicted using silica geothermometers.

In general, the CG system is located within 300 m of the surface in the Quaternary sediments, which contain substantial amounts of calcite and dolomite. Therefore, the chemical

Table 4 Correlation matrix of the physico-chemical water parameters in DGW

Catalog	K^+	Na^+	Ca^{2+}	Mg^{2+}	Cl^-	SO_4^{2-}	HCO_3^-	pH	T	TDS	SiO_2	F^-
K^+	1											
Na^+	0.90**	1										
Ca^{2+}	0.64**	0.55*	1									
Mg^{2+}	0.63**	0.64**	0.81**	1								
Cl^-	0.512*	0.49	0.31	0.25	1							
SO_4^{2-}	0.71**	0.80**	0.57*	0.60*	− 0.09	1						
HCO_3^-	0.57*	0.72**	0.01	0.29	0.22	0.51*	1					
pH	− 0.38	− 0.36	− 0.45	− 0.46	− 0.53*	− 0.10	− 0.11	1				
T	0.20	0.01	− 0.29	− 0.23	− 0.12	− 0.02	0.28	0.10	1			
TDS	0.90**	0.99**	0.59*	0.65**	0.41	0.85**	0.71**	− 0.33	− 0.01	1		
SiO_2	0.45	0.42	− 0.08	0.02	− 0.16	0.50	0.54*	0.28	0.36	0.44	1	
$F-$	− 0.73**	− 0.79**	− 0.6*	− 0.57*	− 0.29	− 0.72**	− 0.57*	0.24	− 0.04	− 0.81**	− 0.21	1

*Significant at the 0.05 level (2-tailed)

**Significant at the 0.01 level (2-tailed)

composition of water in this system is mainly made up of HCO_3–Ca and HCO_3–Ca–Mg types, with low TDS content. Faulting is likely to have provided conduits for some water from the CG system to discharge to and mix with water from the SGW system. Consequently, water in the SGW system has a mixed composition and consists of SO_4–Na and SO_4–HCO_3–Na water types. By contrast, the DGW system is more than 2000 m deep, so the thermal reservoir is closed and the temperatures are high. Under these conditions, there are intense water–rock interactions, which have produced a chemical composition that consists of SO_4–Na and SO_4–Cl–Na water types.

Geothermometry

Geothermometers

Na–K–Mg ternary diagrams (Giggenbach 1988) can be used to estimate geothermal reservoir temperatures, distinguish the equilibrium status, and classify geothermal water into three types: immature water, partially equilibrated water, and fully equilibrated water (Karimi et al. 2017; Pang 2001). The SGW and DGW geothermal samples (except for DGW7) plotted below the equilibrium line in Fig. 8, so they can be mainly classified as immature waters and partially equilibrated waters, respectively. The samples plot close to the Mg corner, suggesting that the thermal waters were in partial equilibrium or re-equilibrated with the host rocks during ascent (Karimi et al. 2017). In addition, this diagram provides evidence that water in the SGW system has been mixed with cold water.

Silica geothermometers depend on various equations that relate temperature to the SiO_2 content of the water whose
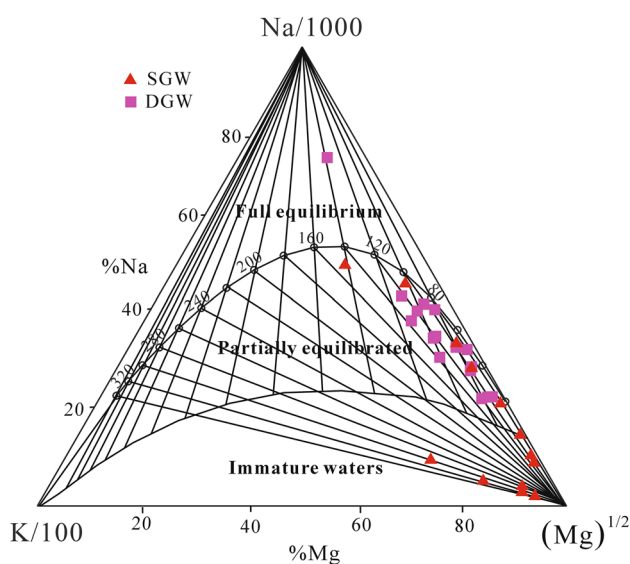

Fig. 8 Na–K–Mg triangular diagram of the geothermal water

temperature is being measured (Ben Brahim et al. 2014). Cation geothermometers depend upon the water–mineral equilibrium of the reservoir (Ben Brahim et al. 2014). In this study, the temperatures of the SGW and DGW systems were obtained by the use of silica and cation geothermometer techniques (Table 5). The different ranges of the geothermometer results are also shown in the Box–Whisker diagram presented in Fig. 9.

There is a large discrepancy between the silica and cation geothermometer results. For the SGW system, the cation geothermometer results deviated by a large margin from the observed values, probably because the water–rock reactions in this system had not reached equilibrium. The range of temperatures for the SGW system that were calculated by the quartz[a] (no-steam loss), quartz[b] (maximum steam loss 100 °C), and the chalcedony methods were 65.5–122.7 °C, 70.7–120.4 °C, and 33.5–94.5 °C, respectively. By contrast, the observed temperatures ranged between 34 and 83.0 °C with an average of 57.5 °C. Therefore, the silica geothermometer results were more reliable for the SGW system, and the chalcedony method was the most reliable, giving estimated temperatures in the range 33.5–94.5 °C.

For the DGW system, temperatures estimated by the quartz[a] and quartz[b] methods were more suitable than those produced by the chalcedony method from the perspective of their distribution ranges. Taking the loss of steam in the process of rising deep geothermal water into consideration, the temperatures measured by the quartz[b] (maximum steam loss 100 °C) could be more reliable and ranged from 94.7 to 140.4 °C, with a relative error of 14.7%. Compared with the results of the K–Mg and Na–K–Ca methods, the temperatures of the DGW system that were found using the Na–K geothermometer were more reliable and mostly ranged from 93.4 to 142.5 °C (except for one sample with an estimate temperature of 78.4 °C). Hence, the temperatures obtained by the quartz[b] and Na–K methods can be taken to provide reasonable estimates for the temperatures in the DGW system.

Multiple mineral equilibrium approach

Multiple mineral equilibrium calculations are another way of estimating the temperature of a thermal reservoir (Ben Brahim et al. 2014; López-Chicano et al. 2001). With this approach, the degree to which water is saturated with respect to a number of mineral phases is examined at different temperatures (Mutlu and Kılıç 2009), and the results are presented in temperature vs. saturation index (SI) diagrams. When values of the SI of one or more mineral phases converge to a value of zero at or around a particular temperature, this temperature can be considered to be the geothermal reservoir temperature (Ben Brahim et al. 2014; Pirlo 2004).

Table 5 Calculated temperatures (in °C) of geothermal water with different geothermometers

Sample ID	Observed	Silica geothermometers			Cation geothermometers		
		Quartz[a]	Quartz[b]	Chalcedony[c]	Na–K[d]	K–Mg[d]	Na–K–Ca[e]
SGW1	42	98.3	99.5	68.1	101.7	55.3	66.6
SGW2	68	97.7	99.0	67.4	98.2	46.9	55.1
SGW3	63	77.6	81.5	46.1	108.1	180.0	69.4
SGW4	34	65.5	70.7	33.5	317.8	78.0	138.9
SGW5	54	82.2	85.5	51.0	269.8	85.5	155.7
SGW6	57	118.5	116.9	89.9	317.8	88.1	168.1
SGW7	61	122.7	120.4	94.5	159.4	313.3	106.0
SGW8	52	70.3	75.0	38.5	82.7	46.9	68.8
SGW9	55	79.8	83.4	48.5	94.9	61.7	96.6
SGW10	57	72.0	76.6	40.3	96.7	73.8	91.5
SGW11	40	66.4	71.5	34.4	94.0	78.3	111.5
SGW12	52	65.5	70.7	33.5	298.2	126.1	203.4
SGW13	51	82.7	86.0	51.6	317.8	108.0	138.1
SGW14	68	77.6	81.5	46.1	317.8	85.6	170.1
SGW15	83	98.2	99.4	68.0	112.4	49.9	70.0
SGW16	55	75.0	79.1	43.4	72.4	51.1	65.7
DGW1	95	121.2	119.2	92.9	102.1	81.9	130.9
DGW2	102	146.4	140.4	120.7	122.9	104.4	165.2
DGW3	94	118.2	116.6	89.6	122.7	97.2	150.6
DGW4	93	113.7	112.8	84.7	101.9	68.1	90.9
DGW5	99	123.4	121.1	95.3	109.3	79.6	198.1
DGW6	91	98.2	99.4	68.0	106.0	95.2	123.0
DGW7	91.5	109.9	109.6	80.6	97.2	298.5	104.7
DGW8	113	113.3	112.4	84.3	127.3	111.8	153.7
DGW9	93	92.8	94.7	62.2	93.4	85.7	91.3
DGW10	95	107.7	107.6	78.2	127.2	99.3	159.6
DGW11	91	95.9	97.5	65.6	131.9	83.6	126.5
DGW12	102	141.9	136.7	115.7	142.5	102.6	144.4
DGW13	94	95.5	97.1	65.2	78.4	66.9	84.8
DGW14	110	100.0	101.0	70.0	138.8	111.8	139.2
DGW15	98	116.7	115.4	88.0	113.4	74.5	114.7
DGW16	91	97.5	98.8	67.2	97.9	74.1	95.4

[a]Fournier and Potter (1982) no-steam loss

[b]Fournier (1977) maximum steam loss 100 °C

[c]Morey et al. (1962)

[d]Giggenbach (1988)

[e]Fournier and Truesdell (1973)

Negative (−) or positive (+) SI values indicate the undersaturation or oversaturation of minerals, respectively.

Based on their observed temperatures, the samples (see Table 1) collected from the SGW system (Sample ID of SGW 1, 2, 3, 10, 15, and 16) and the DGW system (Sample ID of DGW 4, 7, 9, 14, 15, and 16) were selected for assessment using the multiple mineral equilibrium calculation method. The SI values of the major minerals (including albite, Mg-chlorite, chalcedony, fluorite, laumontite, microcline, muscovite, quartz, chrysotile, and anhydrite) for representative thermal water samples are listed in Table 6. In addition, the SI values for these mineral phases were calculated for a range of temperatures (Fig. 10). The temperatures of the SGW and DGW systems mainly ranged from 40 to 100 °C and 75 to 135 °C, with mean values of 70 °C and 105 °C, respectively. The chemical composition of the geothermal waters will have changed with the mixing of cold water and the transformation of the surrounding rock; hence, it is difficult to obtain an accurate thermal reservoir temperature. In general, the mixing ratio of the cold groundwater determined by the mixing model needs to be considered to estimate reservoir temperatures reliably.
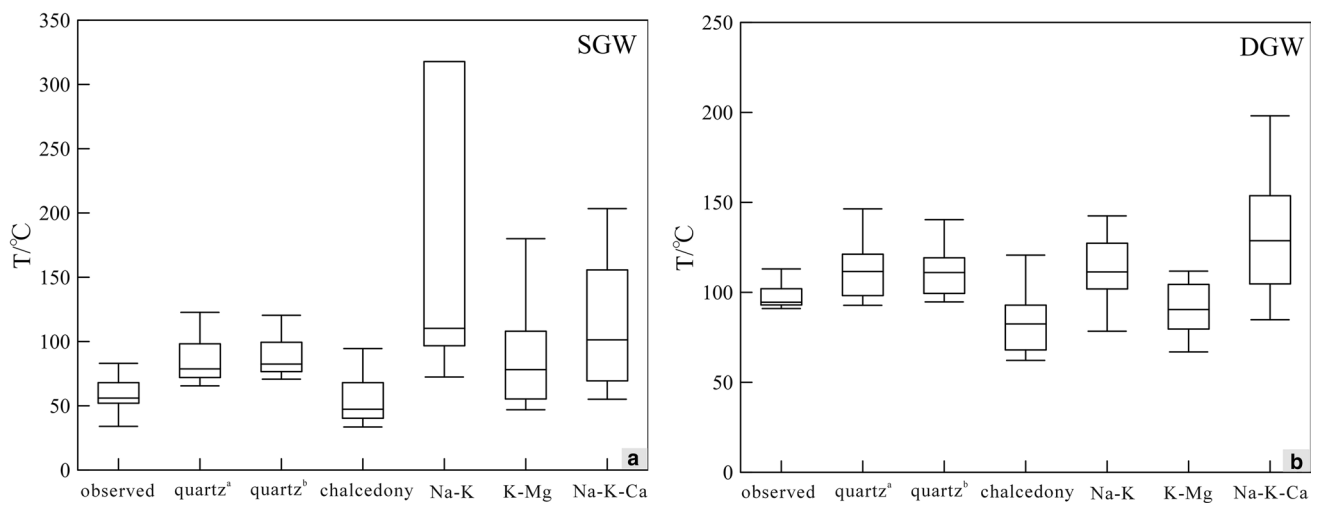
Fig. 9 Box–Whisker diagrams of the silica and cation geothermometer results

Table 6 Mineral saturation indices of representative thermal water samples from the study area

Sample ID	Albite	Mg–Chlorite	Chalcedony	Fluorite	Laumontite	Microcline	Muscovite	Quartz	Chrysotile	Anhydrite
SGW1	− 1.15	− 2.90	− 0.05	0.03	− 0.94	− 0.29	− 0.88	0.25	1.43	− 1.85
SGW2	− 0.74	− 2.01	− 0.05	− 0.44	− 1.13	− 0.48	− 1.50	0.26	2.17	− 2.10
SGW3	− 0.65	− 14.95	− 0.22	− 0.36	− 0.82	− 0.21	− 0.30	0.10	− 6.18	− 2.22
SGW10	− 0.13	− 3.75	− 0.21	− 0.43	− 0.57	0.26	0.60	0.11	0.33	− 1.81
SGW15	− 0.72	3.24	− 0.22	− 0.01	− 0.78	− 0.50	− 1.33	0.07	5.12	− 1.66
SGW16	− 0.37	− 3.88	− 0.15	− 1.19	− 1.05	− 0.21	− 0.29	0.18	0.52	− 2.61
DGW4	− 0.56	− 0.02	− 0.13	0.15	− 1.22	− 0.58	− 2.11	0.15	3.58	− 0.64
DGW7	− 0.67	− 21.38	− 0.15	− 0.18	− 1.68	− 0.71	− 2.22	− 0.32	− 9.23	− 1.43
DGW9	− 0.81	− 3.95	− 0.32	0.15	− 1.47	− 0.91	− 1.79	− 0.04	0.80	− 0.67
DGW14	− 1.10	− 4.50	− 0.37	− 0.19	− 2.58	− 1.24	− 2.83	− 0.13	0.85	− 0.74
DGW15	− 0.44	− 1.23	− 0.12	− 0.09	− 1.25	− 0.42	− 1.51	0.15	2.59	− 0.29
DGW16	− 0.62	− 0.58	− 0.27	− 0.10	− 1.21	− 0.66	− 1.55	0.01	2.90	− 0.70

Silica-enthalpy mixing model

The results of the chemical geothermometers indicate that the ascending geothermal water in the Xi'an geothermal reservoir was generally mixed with cold groundwater along fault structures. The silica-enthalpy mixing model was used to determine the reservoir temperature and quantify the mixing ratios with the cold water (Chatterjee et al. 2016; Li et al. 2018; Wang et al. 2018). It is worth noting that enthalpy rather than temperature is considered in this model, because the combined heat content of two bodies of water at different temperatures are conserved when mixing, but the temperatures are not (Guo et al. 2017).

In Fig. 11, the enthalpy of the DGW system is indicated by point B, where the quartz solubility curve meets the line joining the steam point and point E (representing the mean enthalpies and the SiO$_2$ concentrations of the DGW), indicating that

the DGW system was at a temperature of 108 °C. The trend lines of the shallow geothermal water samples and the cold groundwater were taken as the mixing lines of the CG system (Avsar et al. 2016). Point A, where the mixing line of the CD intersects with the quartz solubility curve, is considered to denote the initial state of the SGW system before mixing, with the estimated values of enthalpy and temperature of 356.4 J/g and 85 °C, respectively. Furthermore, the mixing ratio can be determined by the mixing line between the three points for cold water, mixed geothermal water, and initial geothermal water. The calculation formulae are as follows (Guo et al. 2017):

$$H = \alpha H_{CG} + (1 - \alpha)H_A, \tag{1}$$

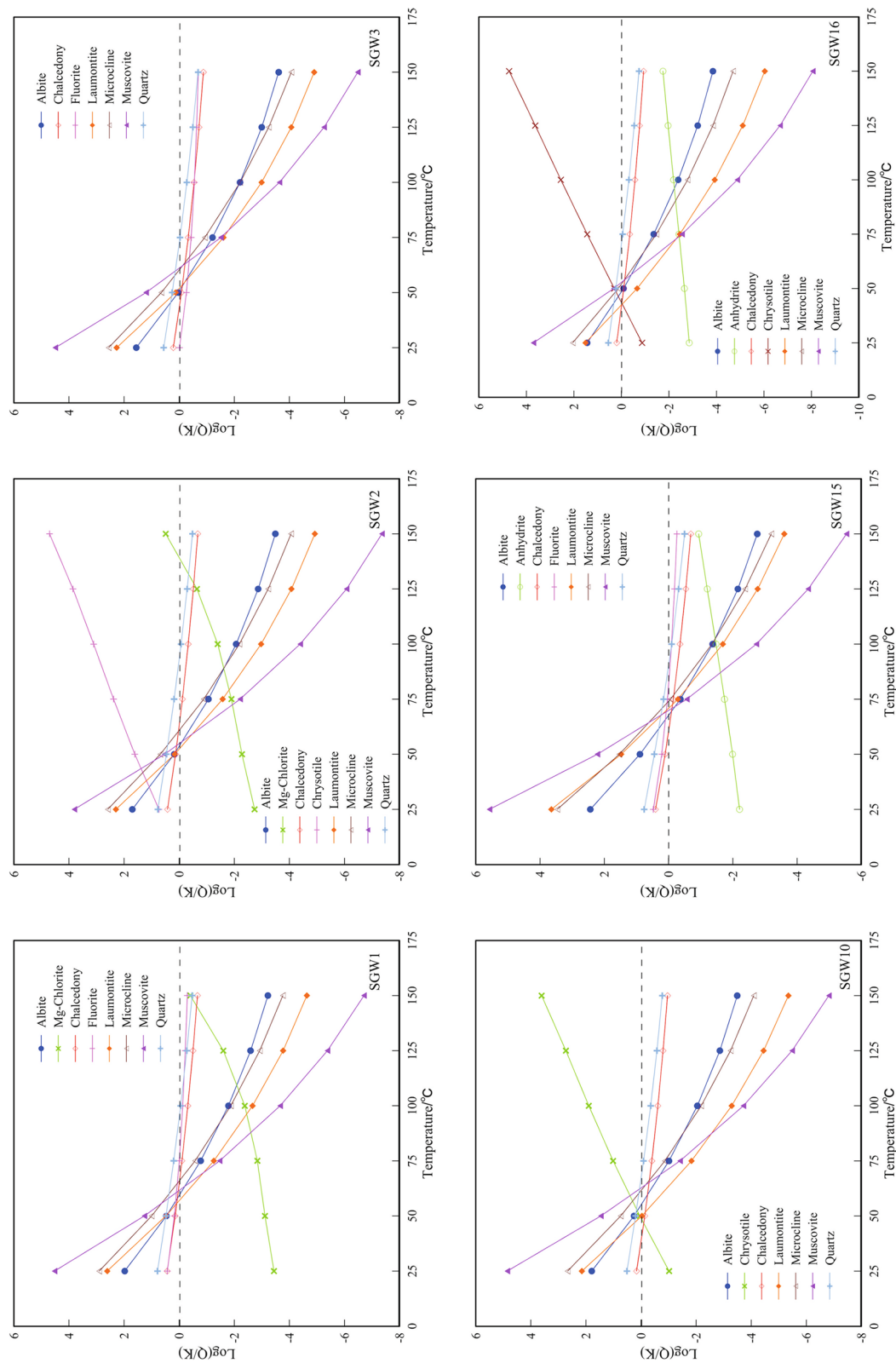$$S = \alpha S_{CG} + (1 - \alpha)S_A, \tag{2}$$

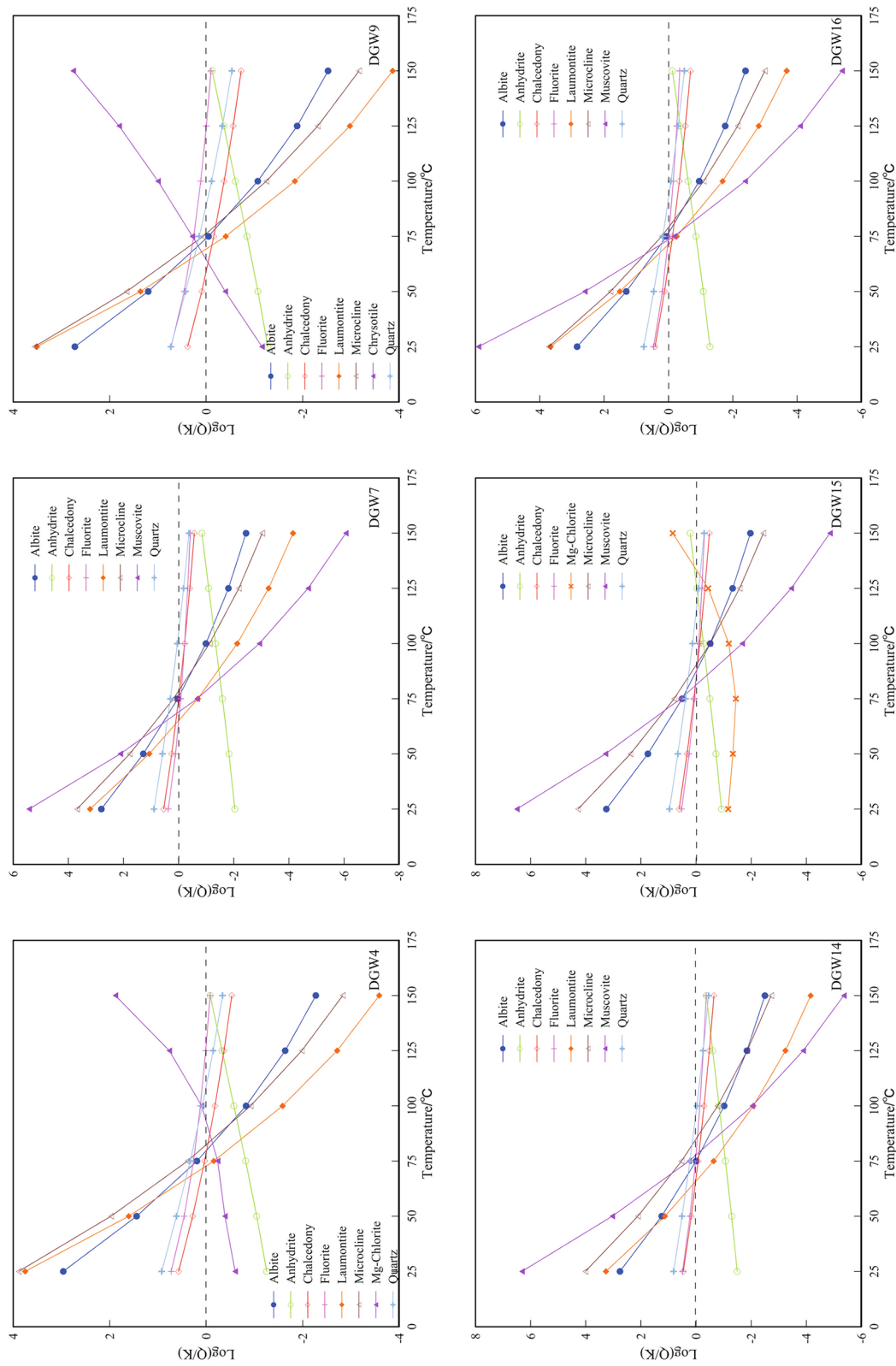**Fig. 10** Mineral equilibrium diagrams for the geothermal water samples
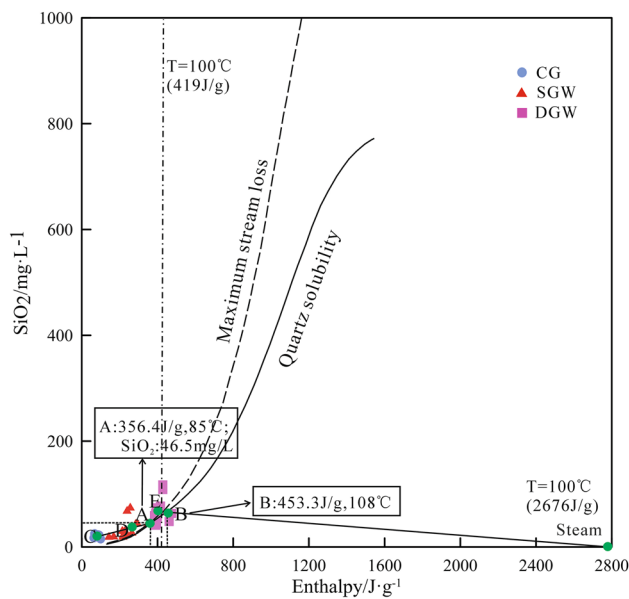
Fig. 10 (continued)

Fig. 11 Silica-enthalpy plot of the geothermal water and cold ground-water. The points C, D, and E represent the mean enthalpies and SiO_2 concentrations of CG, SGW, and DGW, respectively

where H, H_{CG}, and H_A are the enthalpies of SGW, CG, and the initial SGW, S, S_{CG}, and S_A are the SiO_2 concentrations of the SGW, CG, and initial SGW, and α is the mixing ratio of the CG with the initial SGW. These enable the average mixing ratio of cold water with the SGW to be estimated to be approximately 42.7% and 39.4% using the enthalpy values and SiO_2 concentrations, respectively.

Conclusions

An investigation was undertaken to determine the geochemical characteristics and reservoir temperatures of thermal waters in the Xi'an area in the Guanzhong basin in China.

This study and the previous work have indicated that three distinct groundwater systems occur in this geothermal field: an unconsolidated porous-medium Quaternary cold-water reservoir with depths of less than 300 m, belonging to the cold groundwater (CG) system; the Quaternary, Zhangji-apo Group, and Lantian-Bahe Group thermal reservoirs, with depths ranging between 300 and 2000 m belonging to the shallow geothermal water (SGW) system; the Gaoling Group, Bailuyuan Group, and Proterozoic crystalline rock fissure thermal reservoirs with depths of more than 2000 m, representing the deep geothermal water (DGW) system.

The chemical analysis of the water samples from the CG system indicated that the dominant water compositions here are HCO_3–Ca and HCO_3–Ca–Mg, with a low TDS content. The chemical composition of the water in the SGW system consists of SO_4–Na and SO_4–HCO_3–Na types, suggesting

that the water composition was influenced by the effects of the direct or indirect infiltration of precipitation and the effects of cation exchange and adsorption. Water in this system appears to infiltrate along faults which have led to the mixing of water in this system with water from the CG system. Calculations using the silica-enthalpy model suggest that the average mixing ratios of the water from the CG system are 39.4–42.7%. The chemical composition of water in the DGW system was generally of the SO_4–Na and SO_4–Cl–Na types, and was characterized by high temperatures and elevated TDS, F^-, SiO_2, and major ion concentrations. This suggests that water in this system has had a long residence time that has allowed extensive water–rock reactions in a closed geothermal reservoir.

The results of a Q-cluster analysis for a set of water samples collected from the Xi'an geothermal field are consistent with results from the geochemical analysis of the samples, indicating that Q-cluster analysis is a useful classification tool for assessing the nature of the water's chemistry. The associations of the principal variables obtained by the R-cluster method were consistent with the results of the hydrogeochemical assessment of the water quality data.

The reservoir temperature of the SGW system was calculated using the chalcedony geothermometer, indicating that temperatures in this system range from 33.5 to 94.5 °C. The cation geothermometers were not applicable for robustly calculating the temperatures of the SGW system because, as indicated by the Na–K–Mg ternary diagram, this system is not in a state of chemical equilibrium and the water quality has been influenced by mixing processes with an external water source. The temperatures measured by the quartz[b] (maximum steam loss 100 °C) are likely to be more reliable due to the loss of steam in the water rising from this reservoir. Using this method, the temperature of the DGW system was estimated to range from 94.7 to 140.4 °C. The Na–K geothermometer is considered to be a more suitable technique for estimating temperatures in the DGW system, with temperatures in the DGW system estimated to range between 93.4 and 142.5 °C using this method. The multiple mineral equilibrium calculation approach gave temperature estimates of 40–100 °C and 75–135 °C for the SGW and DGW systems, respectively. The silica-enthalpy mixing model yielded average initial temperatures of 85 °C for the SGW system, and 108 °C for the DGW system. The comparison of these geothermometer methods suggests that the temperatures of the SGW and DGW systems are 40–85 °C and 94.7–135 °C, respectively, as determined by comparative analysis using the multiple mineral equilibrium calculation method, the silica-enthalpy mixing model, and the observed data.

This study provides new insights into the analysis of geothermal water by combining hydrogeochemical data and cluster analysis. This approach can be used to study other geothermal systems worldwide. The results from this study

provide guidance for the further assessment and management of the use of geothermal water resources in the Xi'an geothermal field the Guanzhong Basin as a whole. However, the limitations of this study are that it does not apply isotope geothermometers and gas geothermometers to the geothermal discharges, which requires further research.

References

Abdel Moneim AA, Seleem EM, Zeid SA, Abdel Samie SG, Zaki S, El-Fotoh A, A (2015) Hydrogeochemical characteristics and age dating of groundwater in the Quaternary and Nubian aquifer systems in Wadi Qena, Eastern Desert, Egypt. Sustain Water Resour Manag 1(3):213–232

Adam P, Jan D (2008) Application of selected geothermometers to exploration of low-enthalpy thermal water: the Sudetic geothermal region in Poland. Environ Geol 58(8):1629–1638

Arnórsson S (1983) Chemical equilibria in icelandic geothermal systems—implications for chemical geothermometry investigations. Geothermics 12(2):119–128

Avsar O, Gulec N, Parlaktuna M (2013) Hydrogeochemical characterization and conceptual modeling of the Edremit geothermal field (NW Turkey). J Volcanol Geotherm Res 262:68–79

Avsar O, Kurtulus B, Gursu S, Kuscu GG, Kacaroglu F (2016) Geochemical and isotopic characteristics of structurally controlled geothermal and mineral waters of Mugla (SW Turkey). Geothermics 64:466–481

Ben Brahim F, Makni J, Bouri S, Ben Dhia H (2014) Evaluation of temperature and mixing process of water in deep and shallow aquifers in the southwestern Tunisia: case of Djerid region. Arab J Sci Eng 39(7):5677–5689

Chandrajith R, Barth JAC, Subasinghe ND, Merten D, Dissanayake CB (2013) Geochemical and isotope characterization of geothermal spring waters in Sri Lanka: evidence for steeper than expected geothermal gradients. J Hydrol 476:360–369

Chatterjee S, Sharma S, Ansari MA, Deodhar AS, Low U, Sinha UK, Dash A (2016) Characterization of subsurface processes estimation of reservoir temperature in Tural Rajwadi geothermal fields. Maharashtra India Geotherm 59:77–89

Cloutier V, Lefebvre R, Therrien R, Savard MM (2008) Multivariate statistical analysis of geochemical data as indicative of the hydrogeochemical evolution of groundwater in a sedimentary rock aquifer system. J Hydrol 353(3):294–313

Dassi L (2011) Investigation by multivariate analysis of groundwater composition in a multilayer aquifer system from North Africa: A multi-tracer approach. Appl Geochem 26(8):1386–1398

Foued B, Henia D, Lazhar B, Nabil M, Nabil C (2017) Hydrogeochemistry and geothermometry of thermal springs from the Guelma region, Algeria. J Geol Soc India 90(2):226–232

Fournier RO (1977) Chemical geothermometers and mixing models for geothermal systems. Geothermics 5(1):41–50

Fournier RO, Potter RWI (1982) Revised and expanded silica (quartz) geothermometer. Geotherm Resour Counc Bull 11:3–12

Fournier RO, Truesdell AH (1973) An empirical Na–K–Ca geothermometer for natural waters. Geochim Cosmochim Acta 37(5):1255–1275

Giggenbach WF (1988) Geothermal solute equilibria. Derivation of Na–K–Mg–Ca geoindicators. Geochim Cosmochim Acta 52(12):2749–2765

Guo QH, Wang YX (2012) Geochemistry of hot springs in the Tengchong hydrothermal areas, Southwestern China. J Volcanol Geotherm Res 215:61–73

Guo Q, Pang ZH, Wang YC, Tian J (2017) Fluid geochemistry and geothermometry applications of the Kangding high-temperature geothermal system in eastern Himalayas. Appl Geochem 81:63–75

Jiang GM, Wu QC (2009) Study on the sustainable development and utilization of geothermal water resources in Xi'an city. Geol Resour 18(03):210–213 **(in Chinese)**

Karimi S, Mohammadi Z, Samani N (2017) Geothermometry and circulation depth of groundwater in Semnan thermal springs, Northern Iran. Environ Earth Sci 76(19):659

Li PY, Li XY, Meng XY, Li MN, Zhang YT (2016a) Appraising groundwater quality and health risks from contamination in a semiarid region of northwest China. Expo Health 8(3):361–379

Li PY, Wu JH, Qian H (2016b) Preliminary assessment of hydraulic connectivity between river water and shallow groundwater and estimation of their transfer rate during dry season in the Shidi River, China. Environ Earth Sci 75(2):99–114

Li PY, Zhang YT, Yang NA, Jing LJ, Yu PY (2016c) Major ion chemistry and quality assessment of groundwater in and around a mountainous tourist town of China. Expo Health 8(2):239–252

Li J, Yang G, Sagoe G, Li Y (2018) Major hydrogeochemical processes controlling the composition of geothermal waters in the Kangding geothermal field, western Sichuan province. Geothermics 75:154–163

Liu CW, Jang CS, Chen CP, Lin CN, Lou KL (2008) Characterization of groundwater quality in Kinmen Island using multivariate analysis and geochemical modelling. Hydrol Process 22(3):376–383

Liu YP, Zhou X, Deng ZJ, Fang B, Tsutomu Y, Zhao JB, Wang XC (2015) Hydrochemical characteristics and genesis analysis of the Jifei hot spring in Yunnan, southwestern China. Geothermics 53:38–45

López-Chicano M, Bouamama M, Vallejos A, Pulido-Bosch A (2001) Factors which determine the hydrogeochemical behaviour of karstic springs. A case study from the Betic Cordilleras. Spain Appl Geochem 16(9):1179–1192

Lu LH, Pang ZH, Kong YL, Guo Q, Wang YC, Xu CH, Gu W, Zhou LL, Yu DD (2018) Geochemical and isotopic evidence on the recharge and circulation of geothermal water in the Tangshan geothermal system near Nanjing, China: implications for sustainable development. Hydrogeol J 26(5):1705–1719

Lund JW, Boyd TL (2016) Direct utilization of geothermal energy 2015 worldwide review. Geothermics 60:66–93

Ma ZY, Li XC, Zheng HJ, Li JB, Pei B, Guo S, Zhang XL (2017) Origin and classification of geothermal water from Guanzhong Basin, NW China: geochemical and isotopic approach. J Earth Sci 28(4):719–728

Makni J, Bouri S, Ben Dhia H (2013) Hydrochemistry and geothermometry of thermal groundwater of southeastern Tunisia (Gabes region). Arab J Geosci 6(7):2673–2683

Michael K, Golab A, Shulakova V, Ennis-King J, Allinson G, Sharma S, Aiken T (2010) Geological storage of CO2 in saline aquifers—a review of the experience from existing storage operations. Int J Greenhouse Gas Control 4(4):659–667

Mondal NC, Singh VP, Singh VS, Saxena VK (2010) Determining the interaction between groundwater and saline water through groundwater major ions chemistry. J Hydrol 388(1):100–111

Morey GW, Fournier RO, Rowe JJ (1962) The solubility of quartz in water in the temperature interval from 25 to 300 °C. Geochim Cosmochim Acta 26(10):1029–1043

Mutlu H, Kılıç A (2009) Geothermometry applications for the Balıkesir thermal waters. Turk Environ Geol 56(5):913–920

Palandri JL, Reed MH (2001) Reconstruction of in situ composition of sedimentary formation waters. Geochim Cosmochim Acta 65(11):1741–1767

Pang ZH (2001) Isotope and chemical geothermometry and its applications. Sci China Ser E Technol Sci 44(1):16–20

Piper AM (1944) A graphic procedure in the geochemical interpretation of water-analyses. Eos Trans Am Geophys Union 25(6):914–928

Pirlo MC (2004) Hydrogeochemistry and geothermometry of thermal groundwaters from the Birdsville Track Ridge, Great Artesian Basin, South Australia. Geothermics 33(6):743–774

Qin DJ, Pang ZH, Turner JV, Wen XR, Zhao YD, Xu XL, Liu T (2005a) Isotopes of geothermal water in Xi'an area and implication on its relation to karstic groundwater in North Mountains. Acta Petrol Sin(05): 1489–1500 **(in Chinese)**

Qin DJ, Turner JV, Pang ZH (2005b) Hydrogeochemistry and groundwater circulation in the Xi'an geothermal field, China. Geothermics 34(4):471–494

Reed M, Spycher N (1984) Calculation of pH and mineral equilibria in hydrothermal waters with application to geothermometry and studies of boiling and dilution. Geochim Cosmochim Acta 48(7):1479–1492

Sanada T, Takamatsu N, Yoshiike Y (2006) Geochemical interpretation of long-term variations in rare earth element concentrations in acidic hot spring waters from the Tamagawa geothermal area. Jpn Geotherm 35(2):141–155

Swanson SK, Bahr JM, Schwar MT, Potter KW (2001) Two-way cluster analysis of geochemical data to constrain spring source waters. Chem Geol 179(1):73–91

Wang X, Wang G, Lu C, Gan H, Liu Z (2018) Evolution of deep parent fluids of geothermal fields in the Nimu–Nagchu geothermal belt. Tibet China Geotherm 71:118–131

Xu GF (2014) Isotope and hydrochemical evidence of Genetic about deep geothermal water, as the central of guanzhong basin for an example. M.S. Thesis, Chang'an University, Xi'an, China **(in Chinese)**

Yang PH, Cheng Q, Xie SY, Wang JL, Chang LR, Yu Q, Zhan ZJ, Chen F (2017) Hydrogeochemistry and geothermometry of deep thermal water in the carbonate formation in the main urban area of Chongqing, China. J Hydrol 549:50–61

Zhang XD, Qian H, Chen J, Qiao L (2014) Assessment of groundwater chemistry and status in a heavily used semi-arid region with multivariate statistical analysis. Water 6(8):2212–2232

Publisher's Note Springer Nature remains neutral with regard to jurisdictional claims in published maps and institutional affiliations.